npj | climate and atmospheric science

www.nature.com/npjclimatsci

ARTICLE OPEN

Check for updates

Pollution severity-regulated effects of roof strategies on China's winter $PM_{2.5}$

Fan Wang[1], Gregory R. Carmichael[2], Xiaorui Zhang[1], Xiang Xiao[1] and Meng Gao[1]✉

Urbanization took place rapidly over recent decades and is expected to continue in the future, producing a series of environmental issues, including heat stress. Cool roof and green roof strategies have been adopted in a number of megacities to mitigate urban heat and carbon emissions, yet China is lagging behind developed countries in the implementation. One reason is the lack of careful and thoughtful assessment of potential effects of roof strategies, including their influences on winter $PM_{2.5}$. With numerical simulations in this study, we assess how cool and green roof strategies affect winter $PM_{2.5}$ pollution in North China, and we find that adoptions of cool roofs tend to aggravate $PM_{2.5}$ pollution in lightly polluted regions. When $PM_{2.5}$ pollution worsens, the negative effects of cool roofs are likely to be diminished. Green roofs cause less enhancements of $PM_{2.5}$ pollution as a result of inhibited evapotranspiration in winter. We demonstrate that the effects of roof strategies are regulated by pollution severity and conclude that green roofs with suppressed evapotranspiration and thus weaker penalty on winter $PM_{2.5}$ pollution seem to be better choices given the current pollution severity level in China, especially for regions suitable for growth of broadleaf plants.

npj Climate and Atmospheric Science (2022)5:55 ; https://doi.org/10.1038/s41612-022-00278-y

INTRODUCTION

Urban population increased progressively in the past century, with merely 13% in 1900 to 29% in 1950. Projections indicated that global urban population would rise to 70% (~6.3 million) by 2050, doubling the number in 2010[1]. Urbanization creates not purely convenience of living and better access to healthcare, it conversely brings about a series of social and environmental issues[2]. The influences of urbanization on the environment are multifaceted and complex, including air/water pollution, ecosystem, climate, etc., and are felt at various scales[3–7]. Urban areas produce nearly 80% of carbon emissions and substantial amounts of air pollutants[8], contributing significantly to regional/global climate change and posing great threats to public health[9,10]. Different surface properties make cities warmer than surrounding areas, and such thermal gradients create urban heat island (UHI)[11,12] that aggravates heat stress faced by urban residents[13,14].

Urbanization is a product of economic growth, and actions are thus needed to mitigate its adverse impacts and achieve sustainable development. Urban warming, as a key player to worsen UHI, is mainly contributed by increased anthropogenic heat that is released from booming urban residents and enlarged use of cement and asphalt[15,16]. Mitigation measures to lessen the negative impacts of urban warming have been taken around the world[17–21]. Cool roof and green roof strategies are the most widely evaluated measures and have been officially adopted in a number of megacities over past decades[22,23]. Cool roofs are designed with high-albedo materials to reflect more sunlight back to space and thus absorb less heat than standard roofs[24], while green roofs adopt vegetation evapotranspiration to cool the built environment[25]. Both cool and green roofs have been demonstrated effectively to reduce near-surface air temperature (by 1–5 °C)[26–30] and cut the energy consumption (by 10–50%)[31–36] of air conditioning use.

Coupled with potently mitigating UHI and reducing carbon emissions, cool and green roof strategies also change ground-level air quality. They are likely to weaken thermal forcing of land surface to the atmosphere to suppress vertical mixing and dispersion of air pollutants or to affect temperature/radiation-dependent chemical processes[37]. It was reported previously that the applications of cool roofs in Southern California led to a slight rise in $PM_{2.5}$ concentration[38,39]. The influence of cool roofs on O_3 formation varies with time and space. Some studies reported enhanced O_3 concentration by cool roofs due to more reflected solar ultraviolet[38,40], while others presented beneficial effects of reduced temperature and thus declined rates of O_3 formation[30,41,42]. In addition to inhibiting turbulent mixing[43], green roofs add more green space in the city, which creates conditions that favor dispersion and deposition of particles[44–48]. A monitoring experiment confirmed that concentrations of $PM_{2.5}$ above green roof were reduced by up to 14.1% compared with those over bare roof[49].

Although the frequency of extreme haze episodes has declined[50] after the implementation of the Action Plan for Prevention and Control of Air Pollution in 2013, haze events with relatively lower concentrations of $PM_{2.5}$ still occur occasionally in recent years[51]. Aerosol–radiation feedbacks (ARF) cut the amount of downward shortwave radiation (SWD) reaching the ground, reduce the sensible heat flux, and lowers the height of the planet boundary layer (PBLH)[27,52], which act to aggravate severity of haze events in China[53–56]. The influences of ARF vary with multiple factors, including aerosol concentration[57,58], optical properties[59–61], surface albedo, etc. Adoptions of cool roofs and green roofs alter transmission of radiation and modify micro-environment of dispersion and deposition, complicating the effects on air quality. Insights on this topic are of great significance, as cool and green roof strategies are anticipated to play a growingly important role in mitigating side effects of urbanization.

In this study, we consider roof strategies and associated radiative transfer and urban hydrological processes in a coupled

[1]Department of Geography, Hong Kong Baptist University, Hong Kong SAR 999077, China. [2]Department of Chemical and Biochemical Engineering, The University of Iowa, Iowa City, IA 52242, USA. ✉email: mmgao2@hkbu.edu.hk

meteorology-chemistry model, with a focus on exploring their effects on wintertime $PM_{2.5}$ pollution in North China. The study period was selected to cover different stages of a winter haze event and the clean days before the event to represent diverse pollution levels, which offers scenarios that could take place in the near future under air pollution control. We find that the effects of roof strategies are regulated by pollution severity and our results offer useful implications on implementation of roof strategies in China.

RESULTS

Enhanced wintertime $PM_{2.5}$ pollution by adoption of cool and green roofs in North China

Model configurations in this study follow Gao et al.[54], and extensive model evaluations by using surface observations of meteorological variables and air pollutants, atmospheric sounding products, surface aerosol optical depth (AOD) measurements, and satellite AOD, with respect to temporal, spatial, and vertical distributions of aerosols, indicated reliable representation for the 2010 haze event by WRF-Chem. We evaluate the simulation of surface air pollutants (see Supplementary Fig. 1), and the results are consistent with those in Gao et al.[54]. Scattering aerosols dominate, particularly in rural and suburban regions. The mean column integrated single scattering albedo (SSA) at 550 nm suggest that SSA values are relatively lower (<0.835) over urban areas, which is associated with high levels of BC from residential sector in the urban. High SSA over northern areas and south-eastern coastal areas are associated with dust and sea salt aerosol, respectively. Figure 1 illustrates resulting changes in near-ground $PM_{2.5}$ concentration and air temperature due to adoptions of cool roofs and green roofs. As the diurnal variations of the influences of roof strategies are significant only during daytime (Supplementary Fig. 3), we present only daytime results here. Higher albedo of cool roofs tends to aggravate $PM_{2.5}$ pollution during the day in urban areas, with maximum enhancement up to 50 μg m^{-3} (Fig. 1a). When surface albedo increases, reduced surface shortwave net radiation weakens surface thermal forcing to the atmosphere (Fig. 1c) and inhibits vertical development of convective boundary layer[62], leading to an increase in $PM_{2.5}$ concentration. Consistent findings were reported by refs. [38,39] for widespread adoption of cool roofs in southern California. Although albedo does not change in simulation cases of green roofs from actual cases, we observe still an increase of 10–20 μg m^{-3} in $PM_{2.5}$ concentrations in Beijing due to employment of green roofs (see Fig. 1b) because the weak evapotranspiration slightly inhibits the vertical mixing.

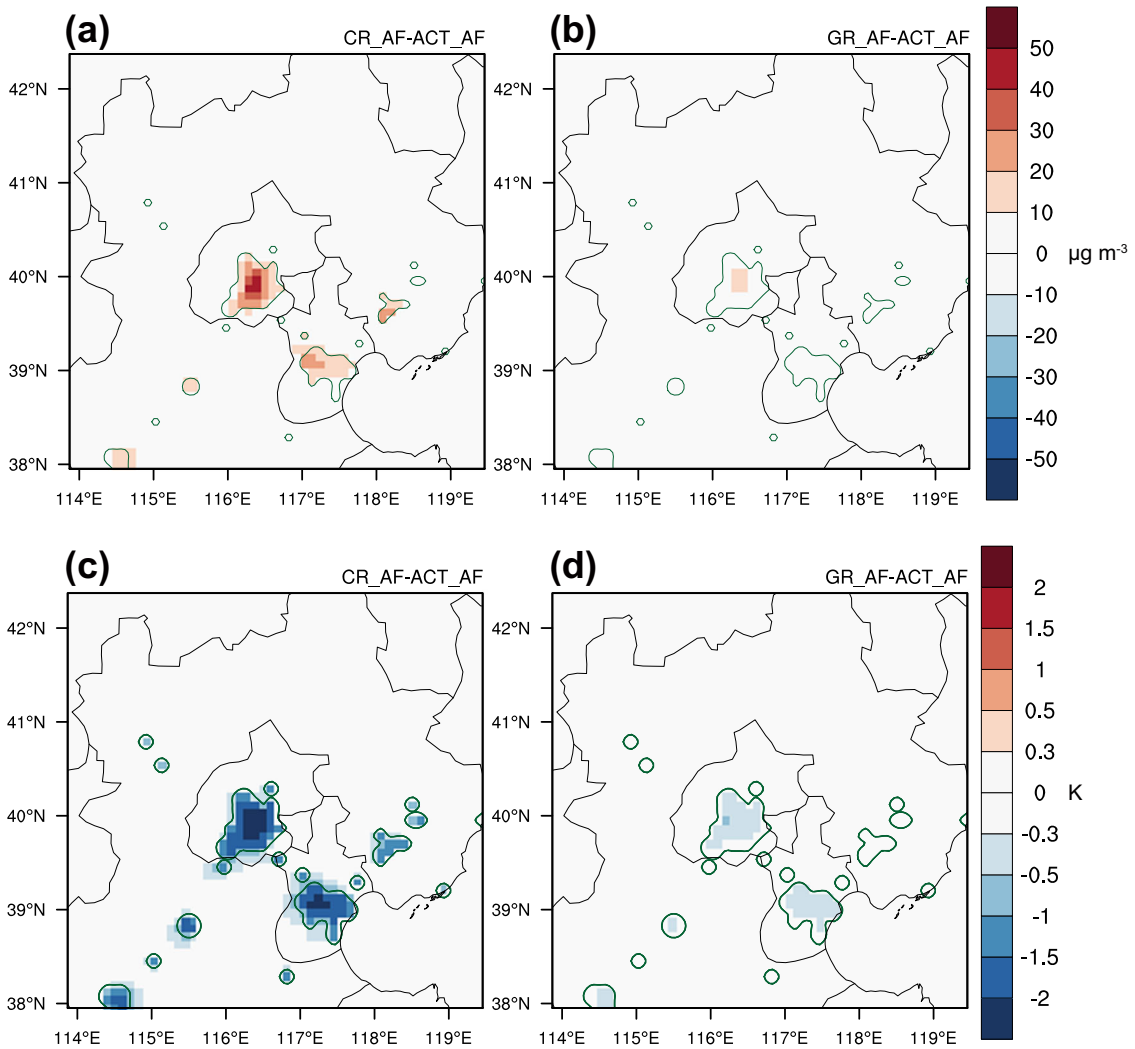

Fig. 1 Spatial features of difference in daytime $PM_{2.5}$ concentration and 2 m air temperature. Difference in daytime (9:00–17:00 LST) **a, b** near-ground $PM_{2.5}$ concentration and **c, d** 2 m air temperature from 14 to 20 January 2010. Green circles represent the locations of urban grids. The impacts of cool roofs are indicated by differences between CR_AF and ACT_AF, while the influences of green roofs are denoted with differences between GR_AF and ACT_AF.

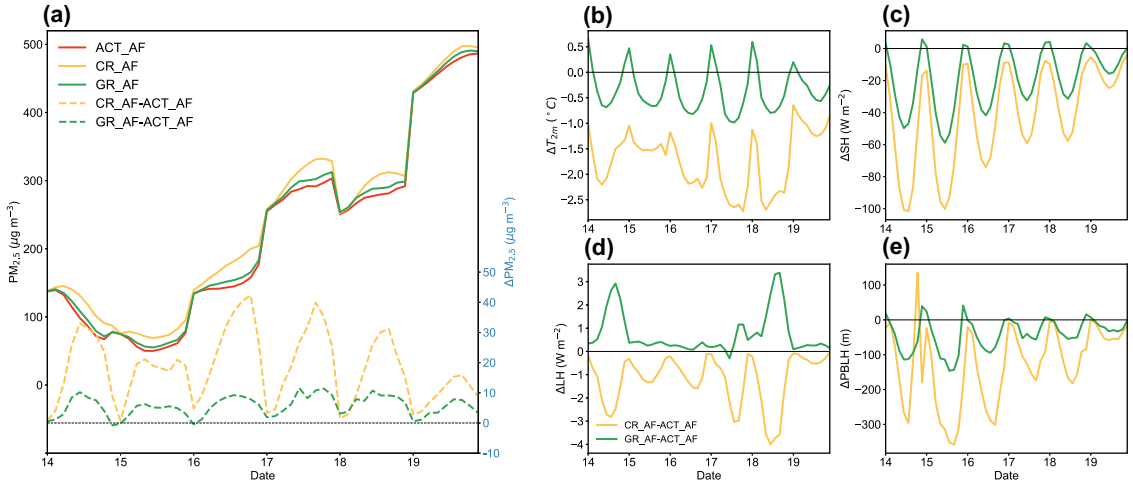

Fig. 2 Trend and variation of $PM_{2.5}$ concentration and related meteorological variables. Difference in daytime (9:00–17:00 LST) **a** near-ground $PM_{2.5}$ concentration and meteorological variables: **b** 2 m air temperature (T_{2m}), **c** sensible heat (SH), **d** latent heat (LH) and **e** planet boundary layer height (PBLH) between CR_AF and ACT_AF, GR_AF and ACT_AF. The left *y* axis of Fig. 2a represents solid lines in the figure; the right *y* axis represents dashed lines.

The effects of roof strategies on $PM_{2.5}$ pollution and the association with pollution severity

Figure 2a suggests that daily variations of changes in $PM_{2.5}$ induced by employment of cool roofs exhibit a negative relationship with pollution severity. On a clean day (15 January), CR results in largest increase in $PM_{2.5}$ concentration (~21 μg m^{-3}, 42%). On light pollution days (14 and 16 January), CR results in the moderate increase in $PM_{2.5}$ (~33 μg m^{-3}, 34% and ~40 μg m^{-3}, 26%). However, a negligible (only ~16 μg m^{-3}, 5%) enhancement is found on severe pollution day (19 January). As $PM_{2.5}$ pollution worsens in urban regions, CR-induced increases in $PM_{2.5}$ concentration are likely to be diminished. Compared with the influences of CR, GR-induced changes of $PM_{2.5}$ concentrations are generally less than 10 μg m^{-3} and display unremarkable association with pollution levels.

Cool roofs directly reduce SWD transferred into land surface and thus modify the development of planet boundary layer (PBL) to affect formation and dispersion of $PM_{2.5}$. Under clear sky conditions, aerosol–radiation interactions affect the amount of SWD reaching land surface[56,60]. On light pollution days, weaker aerosol–radiation interactions under low aerosol loading produce more SWD at land surface, compared to that on severe pollution day (see Supplementary Fig. 4). Under this circumstance, increased surface albedo due to CR causes larger reductions in SWD transferred into land surface and produces greater changes in surface thermal forcing and PBLH (Fig. 2c, e). The resulting changes in micro-environment and decreases in ventilation can reduce dry deposition of particles[39]. We notice that the largest decease of dry deposition velocity (V_d) occurs on the light pollution day (2.5 mm s^{-1}, 16 January, Supplementary Fig. 5).

To eliminate the uncertainty raised by cloud/fog on the severe pollution day (Supplementary Fig. 4), cloud/fog-induced and aerosol-induced reductions of SWD were compared, and we consider 16 January as a reference for cloud/fog-free. From 16 to 19 January, SWD reaching the land surface is reduced by 174 W m^{-2}, with combined influences of cloud/fog and aerosol. When aerosol–radiation interaction is not considered, SWD is reduced by 95 W m^{-2} by cloud/fog, suggesting that aerosol accounts for reductions of 79 W m^{-2}, more than three times of total declines from 16 to 18 January (~23 W m^{-2}). We thus believe that CR induced increase in $PM_{2.5}$ is suppressed with deterioration of aerosol pollution.

The effects of green roofs on urban meteorology and $PM_{2.5}$ pollution are mainly through ambient temperature, constituents of green roof structure and the vegetation properties on the rooftop[63]. As shown in Fig. 2d, evapotranspiration plays a negligible role due to low air temperature (−10 to 5 °C) in winter, and maximum decrease of temperature was accordingly only 0.5–1 K (Fig. 2b). We even observe a slight increase in air temperature after sunrise and before sunset due to release of heat storage (Fig. 2b). Under this circumstance, much smaller decreases of PBLH and increases in near-ground $PM_{2.5}$ concentration are found as the influence of cool roofs. Besides, the treatments of green roofs in our model do not include the changes in deposition processes of particles[64,65] due to adoptions of green roofs, which is likely to compete with the effects of evapotranspiration cooling. Our offline calculation of V_d (see Supplementary Fig. 5) reveals different characteristics on clean days and pollution days. On clean days, the positive values of V_d (GR_AF minus ACT_AF) indicate that green roofs increase dry deposition due to the absorption by plants (concluded from differences in red dashed lines between Supplementary Fig. 5a, b) which is probably caused by higher SWD. While on pollution days, the results indicate that green roofs tend to reduce dry deposition of particles as a result of unfavorable ventilation, while absorption of particles by evergreen needleleaf plants in North China compensate the reduction, although negligibly (differences between Supplementary Fig. 5a, b).

Impacts of adoptions of cool and green roofs on ARF

Figure 3 displays ARF-induced changes in near-ground $PM_{2.5}$ concentration of cool and green roofs, compared with actual conditions. Because the low $PM_{2.5}$ concentration resulting in rare changes on ARF on first two days (not shown), we only show the conditions on following four days. ARF results in consistent increases in near-ground $PM_{2.5}$ concentrations for both ACT and CR conditions (see Supplementary Fig. 6a, b). However, the effects of ARF are inhibited in CR, with decreases of 5–20 μg m^{-3} compared to those for ACT in urban areas. This is because the weaker boundary layer process for the CR suppresses the effects of ARF on PBLH. On the other hand, minimal differences in ARF-induced $PM_{2.5}$ concentration are found for GR, which is also shown in the temporal variation of ARF-induced changes in $PM_{2.5}$ (Fig. 3d). It is worth noting that cool roofs reduce ARF-induced enhancements of $PM_{2.5}$ pollution on heavy (17–18 January) and severe pollution (19 January) days, but increase those on light pollution (16 January) day.

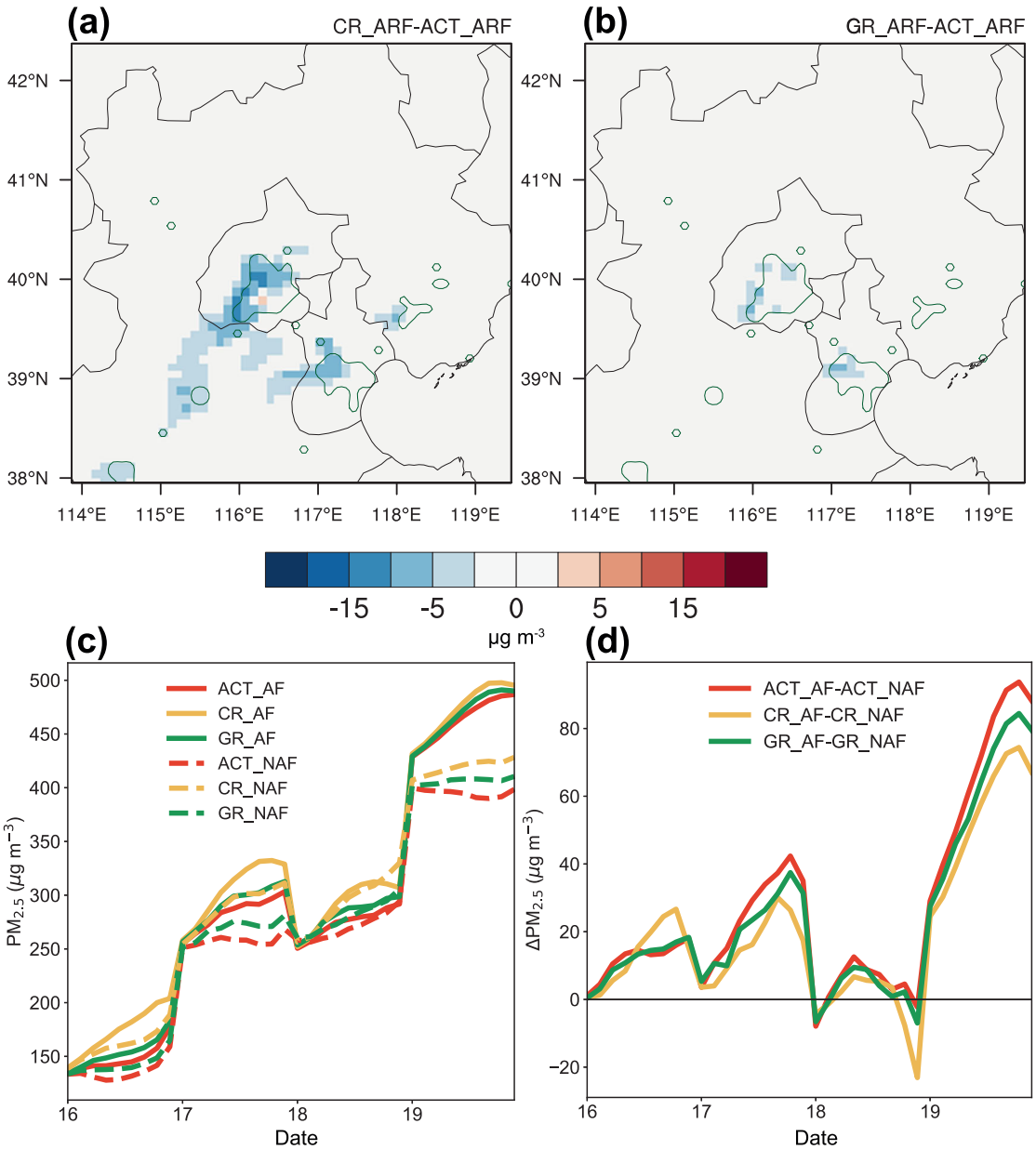

Fig. 3 Spatial and temporal differences in ARF-induced $PM_{2.5}$ concentration. Difference in daytime (9:00–17:00 LST) mean near-ground $PM_{2.5}$ concentration **a** between CR_ARF and ACT_ARF, **b** between GR_ARF and ACT_ARF; temporal variation of daytime **c** near-ground $PM_{2.5}$ concentration and **d** ARF-induced difference.

On light pollution day (16 January), ARF-induced reductions in SWD inferred from ACT, CR, and GR cases are comparable (24%, Fig. 4a). When grid-average albedo of urban areas increases from 0.18 to 0.5 due to implementation of cool roofs, the reductions of PBLH rise from 26% to 41%, leading to larger increase in near-ground $PM_{2.5}$ concentration (Fig. 3d). On heavy pollution days (17–18 January), ARF-induced reductions in SWD are still similar for the three cases (29–30%, Fig. 4a), while ARF-induced changes in PBLH are not notably different (42–46%, Fig. 4a). On heavy pollution days (17–18 January), PBLH exhibits lower values (<200 m) for CR, and vertical mixing occurs mainly at a low altitude, compared with the ACT case (Fig. 4). Lower turbulent diffusivity coefficient (K_m) for the CR case (Supplementary Fig. 7) suppresses the effects of ARF on K_m (Fig. 4c). As a result, 4% greater ARF-induced reductions in PBLH do not cause greater changes in near-ground $PM_{2.5}$ concentration (Fig. 3d). The situation changes on severe pollution day (19 January), when SWD transferring through the atmosphere is largely reduced by extremely high aerosol loading. The increased aerosol loading also strengthens the re-reflection of the upward shortwave from the land surface. Cool roofs reflect more SWD, resulting in more re-reflected shortwave radiation back to the land surface on severe pollution day. This is the main reason why the SWD reaching the land surface reduces less in CR on 19 January (60%, Fig. 4a). Similar to the conditions on heavy pollution days, PBL exhibits even lower values on severe pollution day (Fig. 4c). Under these influences, the ARF-induced reduction on PBLH is weakened (39%), inhibiting the impacts of ARF on accumulation of near-ground $PM_{2.5}$ in CR (Fig. 3d). Green roofs exert an impact on ARF only on 19th January when $PM_{2.5}$ pollution is heaviest. Temperature is the main factor in

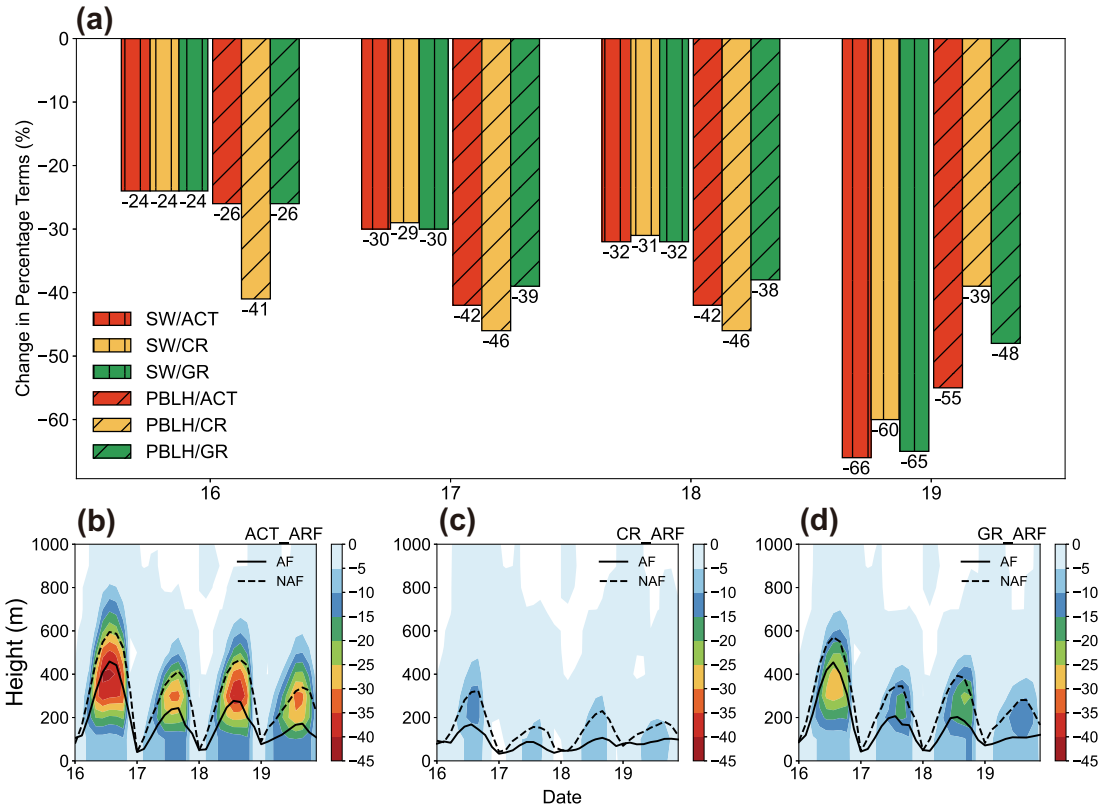

Fig. 4 Variation of aerosol–radiation–PBLH interaction on different pollution days. a Difference in daytime (9:00–17:00 LST) SW and PBLH in percentage terms ((AF-NAF)/NAF × 100%). Turbulent diffusivity coefficient of **b** ACT_ARF, **c** CR_ARF and **d** GR_ARF. The Black lines in **b**, **c**, and **d** represent PBLH.

the influence of green roofs, and ARF causes largest decrease in air temperature when the $PM_{2.5}$ concentration reaches the peak. As a result, we observe notable influence of green roofs on the severe pollution (Fig. 3d).

DISCUSSIONS

With numerical simulations, we assessed how cool and green roof strategies would affect winter $PM_{2.5}$ pollution in North China and ARF processes. The mechanisms were illuminated with analyses of surface energy balance, structure of PBL, and ARF (see Fig. 5). We find that adoptions of cool roofs tend to aggravate $PM_{2.5}$ pollution, while the negative effects are likely to be diminished when pollution worsens. In winter, green roofs cause less enhancements of $PM_{2.5}$ pollution as a result of inhibited evapotranspiration. Besides, cool roofs produce larger effects on ARF in lightly polluted regions, while weaker in heavily polluted regions. We demonstrate that the effects of roof strategies are regulated by pollution severity and our results offer useful implications on implementation of roof strategies in China. Under clean and lightly polluted conditions, green roofs are more beneficial to air quality. For regions suitable for growth of broadleaf plants, absorption of particles by green roofs would further suppress the side effects of green roofs on air quality.

Cool roofs and green roofs were officially prescribed to be installed in a number of megacities, including Tokyo in Japan[66], Chicago and Los Angeles in the United States[22,38] and Toronto in Canada[67]. China is lagging behind[68], and the environmental impacts need more and careful and thoughtful explorations. In cities where aerosol pollution has been successfully controlled[69], applications of cool roof and green roof strategies may not cause serious consequence. For example, Epstein, et al.[38] found an annual average $PM_{2.5}$ increase of $0.19 \pm 0.007\ \mu g\ m^{-3}$. Zhang et al.[39] indicated that cool roofs increased daily average $PM_{2.5}$ concentration by $0.85\ \mu g\ m^{-3}$ in Southern California in summer. In spite of that, cool roofs' effects related to ultraviolet reflection by different materials may aggravate O_3 pollution[38,39,42,43]. China's aerosol pollution has been reduced in recent years, and our examination suggests that daily average increase in $PM_{2.5}$ concentration due to CR in a haze event can be up to $25\ \mu g\ m^{-3}$. Under light pollution and clean scenario with a relatively lower concentration, the enhancement percentage can be even larger, which is anticipated to occur frequently nowadays. Thus, installing cool roofs might not be a good measure in China, given the current pollution severity level. Green roofs with suppressed evapotranspiration and thus weaker penalty on winter $PM_{2.5}$ pollution seem to be better choices, especially for regions suitable for growth of broadleaf plants[70].

We explore in this study the impacts of adopting roof strategies on air quality and ARF from the perspective of surface energy balance, yet the influences of potential resultant reductions on air conditioning and associated emissions are not included. Besides, GR can serve as urban sources of biogenic volatile organic compounds, which might affect ozone pollution and secondary organic aerosol formation. More efforts are thus needed in the future to include these factors to better understand how roof strategies affect air quality. Further studies focusing on more regions and longer time periods are also valuable for better design of urban heat mitigation measures.

METHODS

WRF-Chem model configuration

The Weather Research and Forecasting model coupled with Chemistry (WRF-Chem) version 3.6.1 was employed to simulate dynamic evolution of air pollutants and their interactions with weather[71]. Three domains were

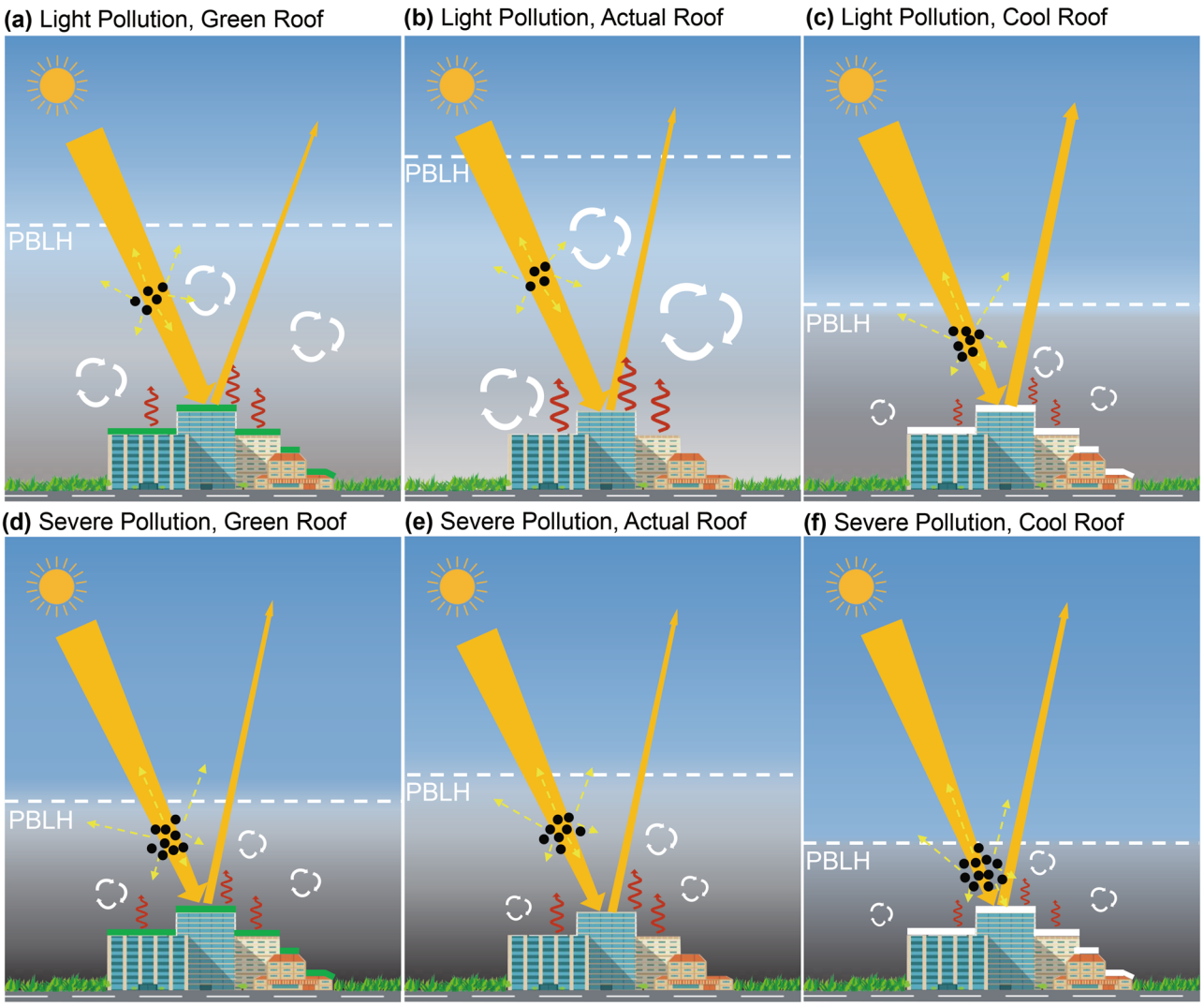

Fig. 5 A conceptual figure of pollution severity-regulated effects of roof strategies on winter $PM_{2.5}$. The conceptual scheme displays interactions between surface energy balance, structure of PBL, ARF, and aerosol concentrations after the applications of cool roofs and green roofs at different pollution levels at daytime. **a** Green roof under light pollution. **b** Actual roof under light pollution. **c** Cool roof under light pollution. **d** Green roof under severe pollution. **e** Actual roof under severe pollution. **f** Cool roof under severe pollution. Orange arrows represent downward solar radiation and that reflected by the surface. Yellow dashed arrows are the reflected and scattered solar radiation by aerosols. Red wavy arrows show the upward forcing of the surface. White dashed lines are the PBLH. White circled arrows represent the turbulent mixing in the PBL. The various shades of background colors mean the different pollution levels.

configured with two-way nesting, and grid resolutions of 81 km, 27 km and 9 km were selected, respectively. The innermost domain covers the entire areas of Beijing and Tianjin, and most regions of Hebei province (see Supplementary Fig. 8). We introduced the Moderate Resolution Imaging Spectroradiometer land cover data in 2010 into simulations to better capture the spatial distribution of different land use types (Supplementary Fig. 8). The 6-h National Centers of Environmental Prediction Final Analysis was used as meteorological initial and boundary conditions. We used the monthly 2010 Multi-resolution Emission Inventory for China (MEIC 2010) offered at $0.25° \times 0.25°$ grids as anthropogenic emissions[72], and online calculated biogenic emissions by the Model of Emissions of Gases and Aerosols from Nature[73]. As biomass burning was not significant in North China during study period[54], we did not include emissions of open biomass burning.

Gas phase and aerosol chemistry were modeled with the Carbon-Bond Mechanism version Z[74] and the 8-bin version of Model for Simulating Aerosol Interactions and Chemistry[75] that includes aqueous chemistry and volatility basis set secondary organic aerosol. Lin cloud microphysics[76] and Grell 3D Ensemble Scheme[77] were employed to simulate aerosol-cloud interactions and precipitation. RRTM[78] and Goddard[79] schemes were used to calculate sub-grid long-wave and short-wave radiation, respectively. Yonsei University planetary boundary layer parameterization[80] was used to simulate boundary layer processes, and we made modifications to output turbulent diffusion coefficient (K_m). Land-atmosphere exchange was simulated using Noah land surface model[81]. Specifically, land-atmosphere exchange in urban grids were calculated by the Urban Canopy Model (UCM)[82], which considers the three-dimensional structure of city and calculates energy balance on the surface of roof, wall and street. The UCM model is a single layer model which has a simplified urban geometry. In UCM, an urban grid will be partitioned into two parts: an impervious fraction and a vegetated fraction, and surface temperature and heat flux of an urban grid cell is an area-averaged temperature and heat flux based on their fractions. The impervious part is further partitioned into two artificial facets in horizontal direction: roof and street, and each has its individual parameters including albedo, emissivity, heat capacity, etc. This enables changing related parameters of the roof to design scenarios for cool roof simulations[83]. We also coupled the module of urban hydrological processes that treats the effects of green roofs to the WRF-Chem model version 3.6.1 as it was officially added after the version of 3.7[65]. It was only employed to calculate the hydrological processes in urban grids of green roofs in the simulation of green roof cases. The evapotranspiration in the model is affected by solar radiation, vapor pressure deficit, air temperature,

Table 1. Descriptions of model simulations.

Experiments	Descriptions
ACT_AF	Roof albedo is set to 0.2; considering ARF.
ACT_NAF	Roof albedo is set to 0.2; not considering ARF; other settings are same as ACT_AF.
CR_AF	Roof albedo is set to 0.9; considering ARF; other settings are same as ACT_AF.
CR_NAF	Roof albedo is set to 0.9; not considering ARF; other settings are same as ACT_AF.
GR_AF	Roof albedo is set to 0.2; fraction of green roof over rooftop is set to 0.8; considering ARF; other settings are same as ACT_AF.
GR_NAF	Roof albedo is set to 0.2; fraction of green roof over rooftop is set to 0.8; not considering ARF; other settings are same as ACT_AF.

(CR_ARF, GR_ARF and ACT_ARF are calculated as the differences between CR_AF and CR_NAF, GR_AF and GR_NAF, and ACT_AF and ACT_NAF, respectively).

and soil moisture[84]. To address the issue of underpredicting sulfate, we added also heterogeneous reactions, following Gao et al.[85]. Besides, a photosynthesis-transpiration scheme (GEM) was employed offline to estimate dry deposition velocity (V_d) of air pollutants[86]. The dry deposition velocity algorithm comprises aerodynamic resistance, laminar boundary-layer resistance and canopy resistance[70,87,88].

Experimental design

We designed three sets of simulations, namely ACT, CR, and GR, to explore the impacts cool and green roofs on ARF and formation of air pollution. The simulation period was from 11 to 20 January 2010 with first three days set up as spin-up time. The first day of the studying period is a light pollution day (14 January), followed by one clean day but with relatively high concentrations (15 January), one light pollution day (16 January), two heavy pollution days (17 and 18 January) and one severe pollution day (19 January). The studying period covered all stages that evolved from clean to severe condition of haze pollution in winter. ACT cases were performed with actual albedo, while CR/GR cases represent the situations with cool/green roofs installed extensively in urban regions. For each set of simulation, aerosol-radiation feedbacks were turned on (AF) and off (NAF). Detailed descriptions of these simulations are shown in Table 1. In ACT and GR cases, the roof albedos were set as default value of 0.2 in UCM. While in CR cases, we set albedo to 0.9 to maximize the impacts of cool roofs on climate and subsequent response in the air pollutants, following Zhang et al.[89]. The albedo of the innermost domain can be seen in Supplementary Fig. 9. The GR cases assumed that the roofs cover 50% of each urban grid and 80% of the roofs in urban areas are vegetation-covered roofs, following Yang et al.[65] and He et al.[90].

DATA AVAILABILITY

All model output data can be obtained from the authors upon request to mmgao2@hkbu.edu.hk.

CODE AVAILABILITY

All codes can be obtained from the authors upon request to mmgao2@hkbu.edu.hk.

Received: 27 February 2022; Accepted: 10 June 2022;
Published online: 04 July 2022

REFERENCES

1. Elmqvist, T. et al. Urbanization, Biodiversity and Ecosystem Services: Challenges and Opportunities. (Springer Nature, 2013).
2. Martínez-Zarzoso, I. & Maruotti, A. The impact of urbanization on CO_2 emissions: evidence from developing countries. *Ecol. Econ.* **70**, 1344–1353 (2011).
3. Han, L., Zhou, W., Li, W. & Li, L. Impact of urbanization level on urban air quality: a case of fine particles (PM(2.5)) in Chinese cities. *Environ. Pollut.* **194**, 163–170 (2014).
4. Kalnay, E. & Cai, M. Impact of urbanization and land-use change on climate. *Nature* **423**, 528–531 (2003).
5. Liu, X. et al. Urbanization effects on observed surface air temperature trends in North China. *J. Clim.* **21**, 1333–1348 (2008).
6. Sun, Y., Zhang, X., Ren, G., Zwiers, F. W. & Hu, T. Contribution of urbanization to warming in China. *Nat. Clim. Change* **6**, 706–709 (2016).
7. Suriya, S. & Mudgal, B. V. Impact of urbanization on flooding: the Thirusoolam sub watershed—a case study. *J. Hydrol.* **412-413**, 210–219 (2012).
8. Chan, C. K. & Yao, X. Air pollution in mega cities in China. *Atmos. Environ.* **42**, 1–42 (2008).
9. Kabisch, N., Korn, H., Stadler, J. & Bonn, A. Nature-Based Solutions to Climate Change Adaptation in Urban Areas: Linkages Between Science, Policy and Practice. (Springer Nature, 2017).
10. Zhu, Y. G., Ioannidis, J. P., Li, H., Jones, K. C. & Martin, F. L. Understanding and harnessing the health effects of rapid urbanization in China. *Environ. Sci. Technol.* **45**, 5099–5104 (2011).
11. Oke, T. R. City size and the urban heat island. *Atmos. Environ.* **7**, 769–779 (1973). (1967).
12. Oke, T. R. The energetic basis of the urban heat island. *Q. J. R. Meteorol. Soc.* **108**, 1–24 (1982).
13. Cao, C. et al. Urban heat islands in China enhanced by haze pollution. *Nat. Commun.* **7**, 12509 (2016).
14. Zhao, L., Lee, X., Smith, R. B. & Oleson, K. Strong contributions of local background climate to urban heat islands. *Nature* **511**, 216–219 (2014).
15. Du, H. et al. Influences of land cover types, meteorological conditions, anthropogenic heat and urban area on surface urban heat island in the Yangtze River Delta Urban Agglomeration. *Sci. Total Environ.* **571**, 461–470 (2016).
16. Theeuwes, N. E. et al. Seasonal dependence of the urban heat island on the street canyon aspect ratio. *Q. J. R. Meteorol. Soc.* **140**, 2197–2210 (2014).
17. Akbari, H., Menon, S. & Rosenfeld, A. Global cooling: increasing world-wide urban albedos to offset CO2. *Clim. Change* **94**, 275–286 (2008).
18. Georgescu, M., Morefield, P. E., Bierwagen, B. G. & Weaver, C. P. Urban adaptation can roll back warming of emerging megapolitan regions. *Proc. Natl Acad. Sci. USA* **111**, 2909–2914 (2014).
19. Krayenhoff, E. S., Moustaoui, M., Broadbent, A. M., Gupta, V. & Georgescu, M. Diurnal interaction between urban expansion, climate change and adaptation in US cities. *Nat. Clim. Change* **8**, 1097–1103 (2018).
20. Li, D., Bou-Zeid, E. & Oppenheimer, M. The effectiveness of cool and green roofs as urban heat island mitigation strategies. *Environ. Res. Lett.* **9**, 055002 (2014).
21. Tan, Z., Lau, K. K.-L. & Ng, E. Urban tree design approaches for mitigating daytime urban heat island effects in a high-density urban environment. *Energy Build.* **114**, 265–274 (2016).
22. Mackey, C. W., Lee, X. & Smith, R. B. Remotely sensing the cooling effects of city scale efforts to reduce urban heat island. *Build. Environ.* **49**, 348–358 (2012).
23. Wang, L., Huang, M. & Li, D. Where are white roofs more effective in cooling the surface? Geophys. Res. Lett. **47**, https://doi.org/10.1029/2020gl087853 (2020).
24. Taha, H., Konopacki, S. & Gabersek, S. Impacts of large-scale surface modifications on meteorological conditions and energy use: a 10-region modeling study. *Theor. Appl. Climatol.* **62**, 175–185 (1999).
25. Oberndorfer, E. et al. Green roofs as urban ecosystems: ecological structures, functions, and services. *BioScience* **57**, 823–833 (2007).
26. Imran, H. M., Kala, J., Ng, A. W. M. & Muthukumaran, S. Effectiveness of green and cool roofs in mitigating urban heat island effects during a heatwave event in the city of Melbourne in southeast Australia. *J. Clean. Prod.* **197**, 393–405 (2018).
27. Jacobson, M. Z. & Kaufman, Y. J. Wind reduction by aerosol particles. Geophys. Res. Lett. 33, https://doi.org/10.1029/2006gl027838 (2006).
28. Morini, E., Touchaei, A., Castellani, B., Rossi, F. & Cotana, F. The impact of albedo increase to mitigate the urban heat island in Terni (Italy) using the WRF model. Sustainability **8**, https://doi.org/10.3390/su8100999 (2016).
29. Roebber, P. J. & Smith, K. R. Green roof mitigation potential for a proxy future climate scenario in Chicago, Illinois. *J. Appl. Meteorol. Climatol.* **50**, 507–522 (2011).

30. Touchaei, A. G., Akbari, H. & Tessum, C. W. Effect of increasing urban albedo on meteorology and air quality of Montreal (Canada)—episodic simulation of heat wave in 2005. *Atmos. Environ.* **132**, 188–206 (2016).
31. Baniassadi, A., Sailor, D. J., Crank, P. J. & Ban-Weiss, G. A. Direct and indirect effects of high-albedo roofs on energy consumption and thermal comfort of residential buildings. *Energy Build.* **178**, 71–83 (2018).
32. Gago, E. J., Roldan, J., Pacheco-Torres, R. & Ordóñez, J. The city and urban heat islands: a review of strategies to mitigate adverse effects. *Renew. Sustain. Energy Rev.* **25**, 749–758 (2013).
33. Kolokotsa, D. D. et al. Cool roofs and cool pavements application in Acharnes, Greece. *Sustain. Cities Soc.* **37**, 466–474 (2018).
34. Macintyre, H. L. & Heaviside, C. Potential benefits of cool roofs in reducing heat-related mortality during heatwaves in a European city. *Environ. Int.* **127**, 430–441 (2019).
35. Oleson, K. W., Bonan, G. B. & Feddema, J. Effects of white roofs on urban temperature in a global climate model. *Geophys. Res. Lett.* **37**, https://doi.org/10.1029/2009gl042194 (2010).
36. Yang, J., Wang, Z.-H. & Kaloush, K. E. Environmental impacts of reflective materials: Is high albedo a 'silver bullet' for mitigating urban heat island? *Renew. Sustain. Energy Rev.* **47**, 830–843 (2015).
37. Taha, H. Modeling the impacts of large-scale albedo changes on ozone air quality in the South Coast Air Basin. *Atmos. Environ.* **31**, 1667–1676 (1997).
38. Epstein, S. A. et al. Air-quality implications of widespread adoption of cool roofs on ozone and particulate matter in southern California. *Proc. Natl Acad. Sci. USA* **114**, 8991–8996 (2017).
39. Zhang, J. et al. Investigating the urban air quality effects of cool walls and cool roofs in Southern California. *Environ. Sci. Technol.* **53**, 7532–7542 (2019).
40. Chen, L., Zhang, M., Zhu, J., Wang, Y. & Skorokhod, A. Modeling impacts of urbanization and urban heat island mitigation on boundary layer meteorology and air quality in Beijing under different weather conditions. *J. Geophys. Res. Atmos.* **123**, 4323–4344 (2018).
41. Han, B.-S., Baik, J.-J., Kwak, K.-H. & Park, S.-B. Effects of cool roofs on turbulent coherent structures and ozone air quality in Seoul. *Atmos. Environ.* **229**, https://doi.org/10.1016/j.atmosenv.2020.117476 (2020).
42. Taha, H. Meso-urban meteorological and photochemical modeling of heat island mitigation. *Atmos. Environ.* **42**, 8795–8809 (2008).
43. Zhong, T., Zhang, N. & Lv, M. A numerical study of the urban green roof and cool roof strategies' effects on boundary layer meteorology and ozone air quality in a megacity. *Atmos. Environ.* **264**, https://doi.org/10.1016/j.atmosenv.2021.118702 (2021).
44. Chen, M., Dai, F., Yang, B. & Zhu, S. Effects of neighborhood green space on $PM_{2.5}$ mitigation: Evidence from five megacities in China. *Build. Environ.* **156**, 33–45 (2019).
45. Deutsch, B., Whitlow, H., Sullivan, M. & Savineau, A. Re-greening Washington DC: a green roof vision based on environmental benefits for air quality and storm-water management. (2005).
46. Gourdji, S. Review of plants to mitigate particulate matter, ozone as well as nitrogen dioxide air pollutants and applicable recommendations for green roofs in Montreal, Quebec. *Environ. Pollut.* **241**, 378–387 (2018).
47. Janhäll, S. Review on urban vegetation and particle air pollution—deposition and dispersion. *Atmos. Environ.* **105**, 130–137 (2015).
48. Speak, A. F., Rothwell, J. J., Lindley, S. J. & Smith, C. L. Urban particulate pollution reduction by four species of green roof vegetation in a UK city. *Atmos. Environ.* **61**, 283–293 (2012).
49. Luo, H., Wang, N., Chen, J., Ye, X. & Sun, Y.-F. Study on the thermal effects and air quality improvement of green roof. *Sustainability* **7**, 2804–2817 (2015).
50. Gao, M. et al. China's emission control strategies have suppressed unfavorable influences of climate on wintertime $PM_{2.5}$ concentrations in Beijing since 2002. *Atmos. Chem. Phys.* **20**, 1497–1505 (2020).
51. Xiao, Q. et al. Changes in spatial patterns of $PM_{2.5}$ pollution in China 2000–2018: impact of clean air policies. *Environ. Int.* **141**, 105776 (2020).
52. Xu, M. et al. Steady decline of east Asian monsoon winds, 1969–2000: evidence from direct ground measurements of wind speed. *J. Geophys. Res.* **111,** https://doi.org/10.1029/2006jd007337 (2006).
53. Ding, A. J. et al. Enhanced haze pollution by black carbon in megacities in China. *Geophys. Res. Lett.* **43**, 2873–2879 (2016).
54. Gao, M. et al. Modeling study of the 2010 regional haze event in the North China Plain. *Atmos. Chem. Phys.* **16**, 1673–1691 (2016).
55. Wu, J. et al. Aerosol–radiation feedback deteriorates the wintertime haze in the North China Plain. *Atmos. Chem. Phys.* **19**, 8703–8719 (2019).
56. Zhao, B. et al. Enhanced $PM_{2.5}$ pollution in China due to aerosol-cloud interactions. *Sci. Rep.* **7**, 4453 (2017).
57. Hong, C. et al. Weakening aerosol direct radiative effects mitigate climate penalty on Chinese air quality. *Nat. Clim. Change* **10**, 845–850 (2020).
58. Zhu, J. et al. Enhanced $PM_{2.5}$ decreases and O_3 increases in China during COVID-19 lockdown by aerosol-radiation feedback. *Geophys. Res. Lett.* **48**, e2020GL090260 (2021).
59. Gao, M. et al. Reduced light absorption of black carbon (BC) and its influence on BC-boundary-layer interactions during "APEC Blue". *Atmos. Chem. Phys.* **21**, 11405–11421 (2021).
60. Li, Z. et al. Aerosol and boundary-layer interactions and impact on air quality. *Natl Sci. Rev.* **4**, 810–833 (2017).
61. Liu, Q. et al. New positive feedback mechanism between boundary layer meteorology and secondary aerosol formation during severe haze events. *Sci. Rep.* **8**, 6095 (2018).
62. Yang, J. & Bou-Zeid, E. Scale dependence of the benefits and efficiency of green and cool roofs. *Landsc. Urban Plan.* **185**, 127–140 (2019).
63. Shafique, M., Kim, R. & Rafiq, M. Green roof benefits, opportunities and challenges—a review. *Renew. Sustain. Energy Rev.* **90**, 757–773 (2018).
64. Cook-Patton, S. C. & Bauerle, T. L. Potential benefits of plant diversity on vegetated roofs: a literature review. *J. Environ. Manag.* **106**, 85–92 (2012).
65. Yang, J. et al. Enhancing hydrologic modelling in the coupled weather research and forecasting–urban modelling system. *Bound. Layer. Meteorol.* **155**, 87–109 (2014).
66. Koyama, T., Yoshinaga, M., Hayashi, H., Maeda, K.-I. & Yamauchi, A. Identification of key plant traits contributing to the cooling effects of green façades using freestanding walls. *Build. Environ.* **66**, 96–103 (2013).
67. Carter, T. & Fowler, L. Establishing green roof infrastructure through environmental policy instruments. *Environ. Manag.* **42**, 151–164 (2008).
68. Dong, J., Zuo, J. & Luo, J. Development of a management framework for applying green roof policy in urban China: a preliminary study. *Sustainability* **12**, https://doi.org/10.3390/su122410364 (2020).
69. Squizzato, S., Masiol, M., Rich, D. Q. & Hopke, P. K. $PM_{2.5}$ and gaseous pollutants in New York State during 2005–2016: spatial variability, temporal trends, and economic influences. *Atmos. Environ.* **183**, 209–224 (2018).
70. Niyogi, D., Alapaty, K., Raman, S. & Chen, F. Development and evaluation of a coupled photosynthesis-based Gas Exchange Evapotranspiration Model (GEM) for mesoscale weather forecasting applications. *J. Appl. Meteorol. Climatol.* **48**, 349–368 (2009).
71. Grell, G. A. et al. Fully coupled "online" chemistry within the WRF model. *Atmos. Environ.* **39**, 6957–6975 (2005).
72. Li, M. et al. Anthropogenic emission inventories in China: a review. *Natl Sci. Rev.* **4**, 834–866 (2017).
73. Guenther, A. et al. Estimates of global terrestrial isoprene emissions using MEGAN (Model of Emissions of Gases and Aerosols from Nature). *Atmos. Chem. Phys.* **6**, 3181–3210 (2006).
74. Zaveri, R. A. & Peters, L. K. A new lumped structure photochemical mechanism for large-scale applications. *J. Geophys. Res. Atmos.* **104**, 30387–30415 (1999).
75. Zaveri, R. A., Easter, R. C., Fast, J. D. & Peters, L. K. Model for Simulating Aerosol Interactions and Chemistry (MOSAIC). *J. Geophys. Res.* **113**, https://doi.org/10.1029/2007jd008782 (2008).
76. Lin, Y.-L., Farley, R. D. & Orville, H. D. Bulk parameterization of the snow field in a cloud model. *J. Clim. Appl. Meteorol.* **22**, 1065–1092 (1983).
77. Grell, G. A. Prognostic evaluation of assumptions used by cumulus parameterizations. *Mon. Weather Rev.* **121**, 764–787 (1993).
78. Mlawer, E. J., Taubman, S. J., Brown, P. D., Iacono, M. J. & Clough, S. A. Radiative transfer for inhomogeneous atmospheres: RRTM, a validated correlated-k model for the longwave. *J. Geophys. Res.: Atmos.* **102**, 16663–16682 (1997).
79. Chou, M.-D., Suarez, M. J., Ho, C.-H., Yan, M. M. H. & Lee, K.-T. Parameterizations for cloud overlapping and shortwave single-scattering properties for use in general circulation and cloud ensemble models. *J. Clim.* **11**, 202–214 (1998).
80. Noh, Y., Hong, S.-Y. & Dudhia, J. A new vertical diffusion package with an explicit treatment of entrainment processes. *Mon. Weather Rev.* **134**, 2318–2341 (2006).
81. Mukul Tewari, N. et al. Proceedings of the 20th Conference on Weather Analysis and Forecasting/16th Conference on Numerical Weather Prediction. pp. 11–15.
82. Chen, F. et al. The integrated WRF/urban modelling system: development, evaluation, and applications to urban environmental problems. *Int. J. Climatol.* **31**, 273–288 (2011).
83. Kimura, F. & Kusaka, H. Thermal effects of urban canyon structure on the nocturnal heat island: numerical experiment using a mesoscale model coupled with an urban canopy model. *J. Appl. Meteorol.* **43**, 1899–1910 (2004).
84. Chen, F. & Dudhia, J. Coupling an advanced land surface–hydrology model with the Penn State–NCAR MM5 modeling system. Part I: model implementation and sensitivity. *Mon. Weather Rev.* **129**, 569–585 (2001).
85. Gao, M. et al. Improving simulations of sulfate aerosols during winter haze over Northern China: the impacts of heterogeneous oxidation by NO_2. Front. Environ. Sci. Eng. **10**, https://doi.org/10.1007/s11783-016-0878-2 (2016).
86. Charusombat, U. et al. Evaluating a new deposition velocity module in the Noah Land-Surface model. *Bound. Layer. Meteorol.* **137**, 271–290 (2010).

87. Niyogi, D. D. S., Alapaty, K. & Raman, S. A photosynthesis-based dry deposition modeling approach. *Water, Air, Soil Pollut.* **144**, 171–194 (2003).
88. Wesely, M. Parameterization of surface resistances to gaseous dry deposition in regional-scale numerical models☆. *Atmos. Environ.* **41**, 52–63 (2007).
89. Zhang, J., Zhang, K., Liu, J. & Ban-Weiss, G. Revisiting the climate impacts of cool roofs around the globe using an Earth system model. Environ. Res. Lett. **11**, https://doi.org/10.1088/1748-9326/11/8/084014 (2016).
90. He, C. et al. Cool roof and green roof adoption in a metropolitan area: climate impacts during summer and winter. *Environ. Sci. Technol.* **54**, 10831–10839 (2020).

ACKNOWLEDGEMENTS

The authors would like to acknowledgement the funding support from Research Grants Council of the Hong Kong Special Administrative Region, China (project no. HKBU22201820 and HKBU12202021) and National Natural Science Foundation of China (No. 42005084).

AUTHOR CONTRIBUTIONS

The study was conceived by M.G., and F.W. conducted simulations and data analysis. F.W. and M.G. wrote the paper with inputs from G.R.C., X.Z., and X.X.

COMPETING INTERESTS

The authors declare no competing interests.

ADDITIONAL INFORMATION

Supplementary information The online version contains supplementary material available at https://doi.org/10.1038/s41612-022-00278-y.

Correspondence and requests for materials should be addressed to Meng Gao.

Reprints and permission information is available at http://www.nature.com/reprints

Publisher's note Springer Nature remains neutral with regard to jurisdictional claims in published maps and institutional affiliations.